

Multiaxial fatigue analysis for the shaft of a 100 MW hydro-power generator

C. A. Mantilla¹, J. A. Valdés² and F. Casanova²

¹CELSIA

Calle 15 # 29B-30, Autopista Cali-Yumbo, Cali, COLOMBIA

²School of Mechanical Engineering, Universidad del Valle

Calle 13 # 100-00, Cali, COLOMBIA

Phone: +5723212100 ext 7349; Fax: +5723334899

*Email: gonzalo.casanova@correounivalle.edu.co

ABSTRACT

This paper presents the stress analysis and the corresponding fatigue life prediction for the shaft of a 100 MW hydro-generator. Normal and shear stresses were measured at the cylindrical section of the shaft while generating at several power levels. A finite element model based on the actual loading was developed to verify the points with stress concentration, and determining the corresponding stress concentration factor. Analytical models taken from the literature were implemented to calculate stresses during transient events as phase-to-ground and phase-to-phase failures. The generation history of the machine, obtained by hourly recording the power during one year, was linked with the corresponding stresses to obtain the stress history. This stress history was used along with the Wang-Brown multiaxial fatigue model and the Miner's rule to estimate the fatigue life of the shaft. Stresses on the shaft were found to be dependent on the generated power. Operation at partial load (between 30 and 60% of full load) was found to produce higher vibration in comparison with operation at power greater than 60% of full load. Changing the power level produced higher damage than the vibration produced during operation at a steady state condition. It was found that the shaft has a practically infinite life, even when considering the damage produced during electrical failures.

Keywords: Fatigue life; damage; multiaxial stress; hydro-generator; stress measurement.

INTRODUCTION

Hydropower plants are among the largest sources of electric energy around the world. The rotating parts of the generating equipment are subjected to mechanical stresses that are produced mainly by magnetic pulling forces, centrifugal forces, weight of the components, thermal stresses, and torque applied by the turbine, which is balanced with the electrical, or air-gap torque. Some of those stresses are fluctuating in time and may produce fatigue failure with catastrophic consequences. Most of the structural or failure analyses for the components of a generator have been focused on the shaft. Momcilovic et al. [1] reported the failure analysis of a 28 MW Kaplan shaft where fatigue cracks were detected. In addition to visual examination and material properties analysis, the authors performed stress analysis during

start-up cycles, shut-down cycles, and steady state operation using the Finite Element Method (FEM). They found that the combination of high stress and a corrosive environment on the cracked region caused the failure. A fatigue case of failure for a wind turbine shaft was reported by Zhang [2]. In this case, material properties analysis and analytical stress analysis allowed the authors to conclude that high stress concentration and the scratches, produced by the rubbing with an annular ring, were the main interacting factors causing the failure. Several papers have studied the transient conditions of the shaft torque generated during electrical system faults, and have evaluated their effect over the shaft's fatigue strength [3-6]. Dorji and Ghomashchi [7] presented a literature review about failure mechanisms focused mainly on turbines, where problems such as erosion and cavitation were reported as the main causes of failure. Liu and co-workers reviewed fatigue failures of hydro turbines [8], and analyzed the effect of steady state operation and transient events, over the fatigue life. Gagnon et al. [9] presented a fatigue analysis applied to a turbine runner including high and low stress fluctuations and different crack geometries. Although the stresses on a generator and the methodology to obtain them should be well known to designers, this information is not always shared with the power plant staff. However, power plant engineers need that information to be able to predict the fatigue, or the remaining life for their machines according to the actual operating conditions, and to set up more efficient monitoring, maintenance, replacement, and risk management plans.

In our previous work, a fatigue analysis was developed for the bolts used to connect the runner to the shaft of a 8 MW hydropower machine [10]. In the present manuscript, we developed a stress analysis and fatigue life estimation for the shaft of the rotor of a 100 MW hydropower plant, considering actual working conditions.

METHODOLOGY

The major general features of the methodology are outlined as follows. It included stress experimental quantifications using field strain measurements on the shaft's cylindrical section. Normal and shear stresses on the shaft were measured with the machine operating at different power levels. Operation damage during transient conditions was taken into account by calculating the torque during phase-to-ground (PG), and phase-to-phase (PP) failures using the mathematical models taken from literature [11]. These transient conditions are relevant for the analyzed unit, since it has experienced 13 PGs during the last 30 years of operation. Finite element models of the shaft were used to calculate the critical points with the highest stresses and the stress concentration factors at those points. Using the stresses and the power generation history, a stress history was obtained and used to calculate fatigue life by following the Wang and Brown multiaxial fatigue approach [12].

Geometry

The basic representation of the rotor is presented in Figure 1. The structural parts of the rotor are the runner, shaft, rotor spoke, rotor rim, and the magnetic poles. Figure 2 shows the geometry and general dimensions of the shaft. The shaft is formed by two parts, a turbine shaft and a rotor shaft connected by 18 M76X6 bolts. Bolts of the same size and grade are also used to assemble the rotor spoke and the runner to the shaft.

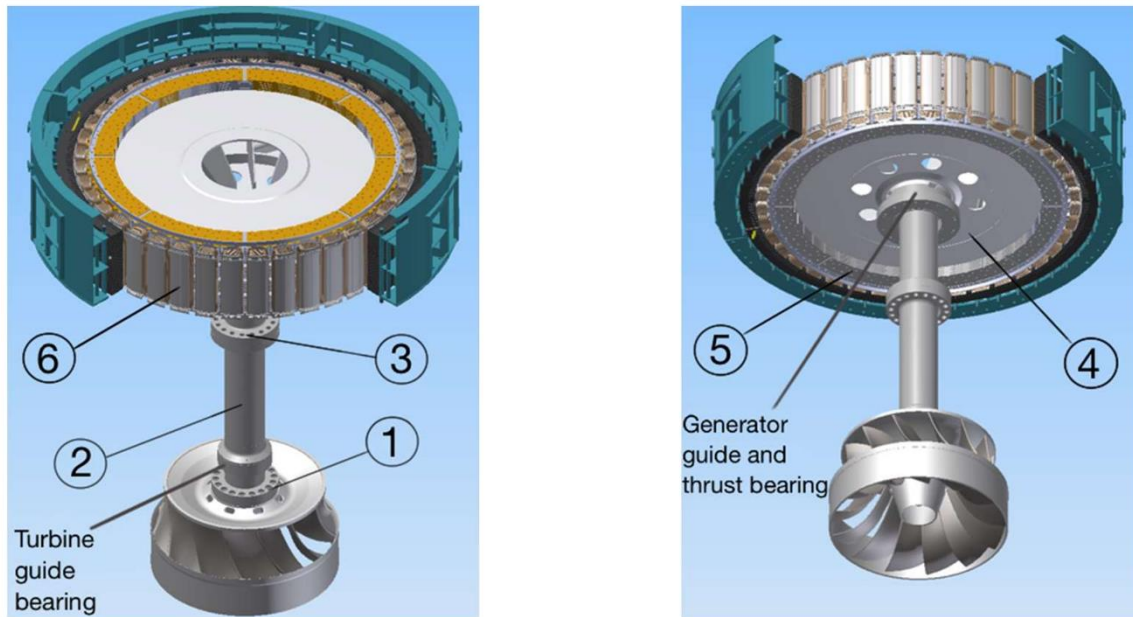


Figure 1. Rotor of the generator showing the main structural elements: 1) runner-shaft connecting bolts, 2) shaft, 3) upper-lower shaft connecting bolts, 4) rotor spoke, 5) rotor rim, and 6) magnetic pole. (Diameter of the rotor=6.8 m).

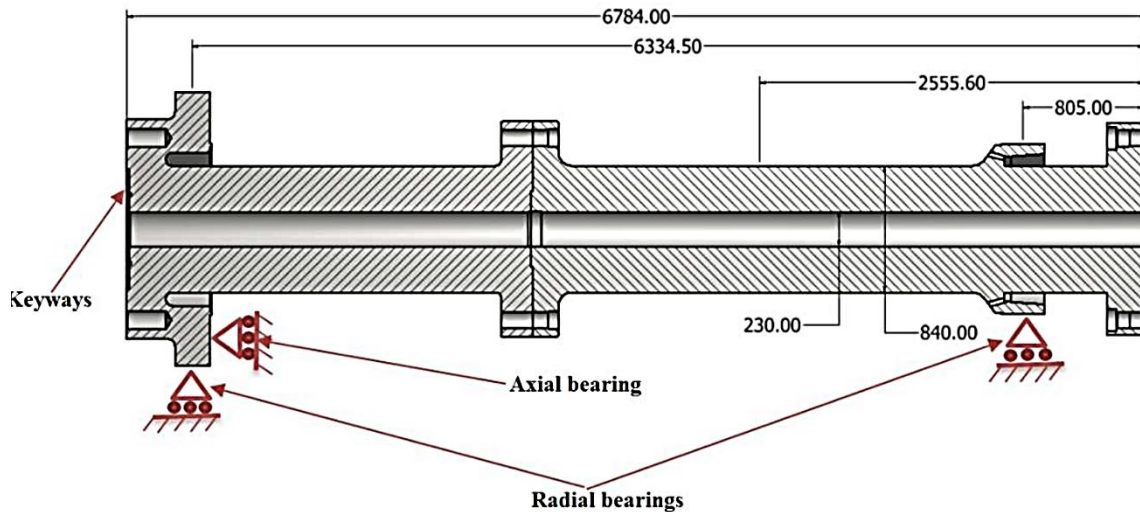


Figure 2. Rotor shaft (left) and turbine shaft (right). Dimensions are in millimetres.

Strain measurement on the turbine shaft

Normal and shear strains on the shaft were measured using strain gauges (DEA-06-250US-350, Micro Measurement, Malvern, PA). A Torque Track 10K system and a Torque Track 9000 system (Biensfeld Engineering, Maple City, MI) were used to transfer the normal and shear strain signals, respectively. The voltage signals from these systems were registered using a 12-bit data acquisition system (model PMD 1280-LS, Measurement Computing, Norton, MA) at a sampling frequency of 100 Hz. Strains were measured with the machine operating at 30, 35, 40, 45, 50, 60, 70, 80, 90, 95, and 100 MW. In addition, strains were

registered during start-up of the machine and during load rejection events from 100 MW. Using the measured strains, stresses were calculated using the plane stress equations.

In general, measured axial strain may be produced by an axial force and a bending moment applied on the shaft [10]. Assuming a constant position of the bending moment, the strain fluctuates with a frequency equal to the frequency of rotation of the shaft (3 Hz). Therefore, the bending moment was calculated from the 3 Hz component of the normal strain signal, and the axial force was calculated from the difference between the total axial strain and the 3 Hz component. Using the basic strength of materials equation, the bending moment was calculated with Eqn. (1):

$$M = \frac{E\varepsilon_b I}{r} \quad (1)$$

where E is the Young modulus, ε_b is the 3 Hz strain component, I is the moment of inertia of the shaft, and r is the radius of the shaft.

Signals for such variables as electrical power, angular velocity, wicket gate position, draft tube pressure pulsations, penstock pressure pulsations, temperature, rotor field current, rotor field voltage, stator terminal current, stator terminal voltage, bearings temperature, stator temperature and control parameters of the unit (Speed governor and voltage regulator) were monitored during the field tests. These signals were registered using a National Instruments (NI) data acquisition system (NI cDAQ-9188), with an analog current input module NI 9203 (input of 20 mA, 16-bit resolution, and sample frequency 100 Hz), and a voltage input module NI 9201 (input of 10 V, 12-bit resolution and sample frequency of 100 kS/s). The NI acquisition system was coupled with the native sensors of the unit to obtain the data during test. All native sensors of the unit had output signals of 4-20 mA or 0-10 V.

Electrical power, angular velocity and wicket gate position measurements were important in order to link the measured strains with the electricity generation. Pressure pulsations of the draft tube and the penstock were also relevant to fit in the model of Turbine-Penstock that was used to model the electrical torque failure. All of the other variables were monitored only for supervision of the machine during tests. Therefore, their results are not included in this manuscript.

Finite element model

A Finite Element Model (FEM) of the shaft was developed to obtain the stress concentration factor at those regions with geometry different from the uniform circular cross section region. The stress concentration factors were used to scale all the stresses measured during the field test and obtain the actual stresses at the notches at different regimes of operation. Even though the shaft is formed by two pieces, namely the turbine shaft and the generator shaft, the shaft was taken as a one-piece element for the analysis applied and described in this section. Figure 3 presents the load and boundary condition of the model labelled as follows: a) compression restriction at the surface of contact with the rotor spoke, b) cylindrical support with restriction for radial displacements (radial bearings), c) displacement support with restriction in the axial direction (thrust bearing), Gw) rotor weight, n) angular speed, g) gravitational effects included, T) mechanical torque, Ht) hydraulic thrust including runner weight. The loads are shown in Table 1. These loads include the average values registered

during the field test measurements for 95 MW load generation. Weight variables were taken from CAD models and reviewed with manufacturer manuals.

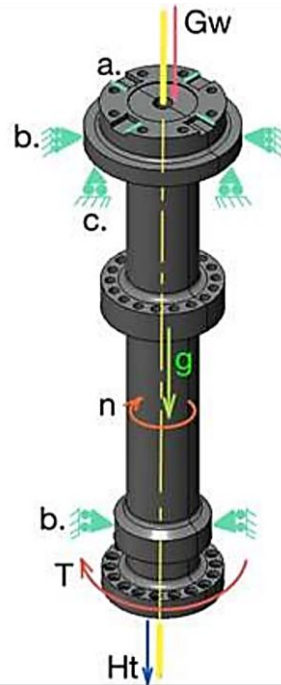


Figure 3. Loads and boundary conditions of the FEM of the shaft.

Table 1. Loads used on the FEM of the shaft.

| Load condition | Value |
|------------------------------|-------|
| Rotor weight – Gw (MN) | 1.89 |
| Angular speed – n (RPM) | 180 |
| Mechanical torque – T (MN-m) | 5.6 |
| Hydraulic thrust – Ht (MN) | 9.4 |
| Runner weight – (MN) | 0.245 |

Analytical models for transient electric failures

Following the methodology of Kirschbaum [11], analytical models to represent the torque for transient phenomena of electrical failures were used, coupled with the mathematical model of the penstock-turbine of Mantilla and co-workers [13]. To couple these models, Euler's equation of angular motion was used [14] modeling the dynamic balance between mechanical and electrical torques. The electrical failure torque (T_e) related to stator insulation failure and its mathematical relations were analyzed for PG and PP failures. Each equation produces results per-unit (PU) dynamic air-gap failure torque, as the ratio between

the air-gap torque and the nominal torque of the machine at full load [11]. To couple the electrical failure torque with the turbine-penstock dynamic response, dynamic turbine penstock equations were implemented according to [13].

As mentioned above, the coupling of the torque at the shaft during failures with the dynamic response of the penstock-turbine system was performed by using Euler's equation of angular motion in the longitudinal direction of the shaft. To model the transient phenomena, the rotor-turbine system was assumed as two degrees of freedom system (Figure 4), which can be modelled as Eqn. (2):

$$\begin{bmatrix} I_t & 0 \\ 0 & I_r \end{bmatrix} \begin{bmatrix} \ddot{\theta}_1 \\ \ddot{\theta}_2 \end{bmatrix} + \begin{bmatrix} k & -k \\ -k & k \end{bmatrix} \begin{bmatrix} \theta_1 \\ \theta_2 \end{bmatrix} = \begin{bmatrix} -T_m \\ T_e \end{bmatrix} \quad (2)$$

where k is the elastic constant of the shaft, which is equal to $k = GJ/L = 570 \text{ MN-m}$; G is the shear modulus; J is the polar moment of inertia; L is the length of the shaft; I_t is the moment of inertia of the turbine (50904 kg-m^2); I_r is the moment of inertia of the rotor (1789867 kg-m^2); θ_1 and θ_2 are the angular displacements produced by the runner and rotor, respectively. Meanwhile, $\ddot{\theta}_1$, $\ddot{\theta}_2$, represent the angular accelerations produced by the runner and rotor, respectively; and T_m , T_e are the mechanical torque and electrical torque, respectively. After solving the previous equation system using the Runge-Kutta method, the torque at the shaft was calculated with Eqn. (3):

$$T = k(\theta_2 - \theta_1) \quad (3)$$

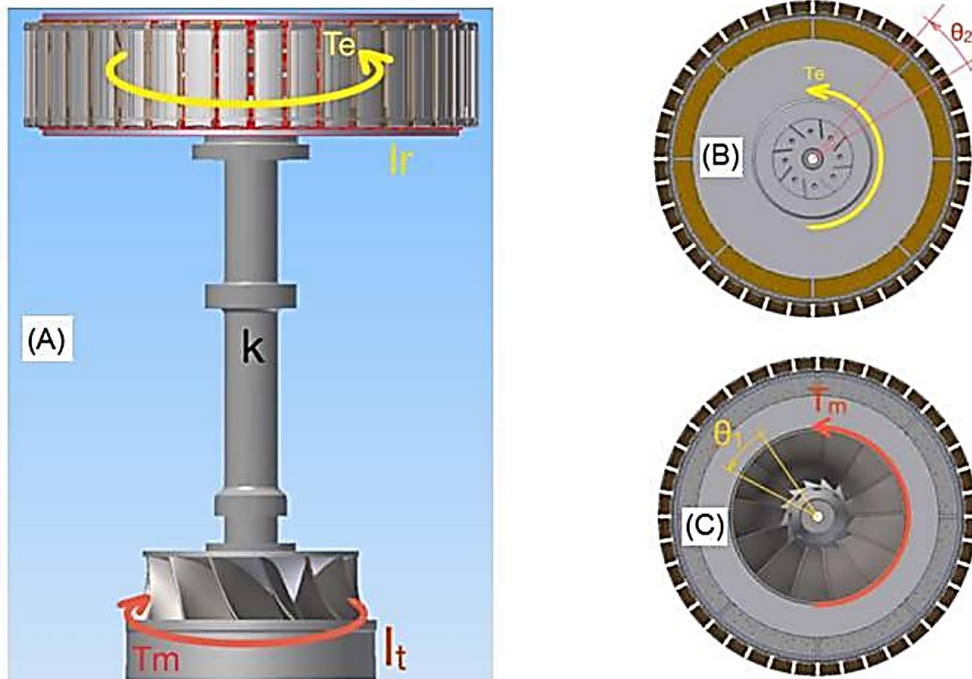


Figure 4. Two degrees of freedom dynamical system of the rotor: (A) lateral view, (B) top view and (C) bottom view.

Fatigue life calculations

Based in the methodology of our previous work [10], a stress history was obtained by linking the power generation history with the stresses at the critical point. The power generation history of the unit was the hourly data of generation (Active power), collected between June of 2014 and June of 2015 (1 MW resolution). As measured loads consisted of an average value and small load variations at each power level due to vibrations, the average load values were linearly interpolated and fitted to the power history to obtain a stress history corresponding to every change of generated power level in the unit. With this stress fluctuation, the fatigue damage corresponding to the Change of Power Level (CPL) of generation during the entire year was calculated. Separately, the fatigue damage per unit hour corresponding to the load fluctuations induced by the vibrations was calculated using the measurements obtained with the machine working in steady state at a constant power level. The damage due to vibrations corresponding to power levels where loads were not measured, were assumed equal to the damage of the immediately higher measured power level (i.e., the damage due to vibrations at 67 MW was assumed the same as the damage at 70 MW). The damage due to vibrations at every power level during the entire year was obtained as the product of the damage per hour and the number of hours worked at the corresponding power level [10]. Damage due to vibration for 100 MW was not accounted for since the machine did not work at power levels greater than 95 MW during the year.

Surfaces should be polished prior to the bonding of the strain gauges. However, the surface at the notch was not polished and consequently, the stresses at that location were corrected by a factor of $\frac{1}{C_a}$ where C_a is the surface correction factor of the fatigue endurance limit for machined surface. A value for this factor of 0.76 was taken according to Norton [15]. Based on the work of Joyce and Lambrecht [16], the total damage during one year of normal operation was calculated as the sum of the damage due to CPL plus the damage produced by vibrations. Additionally, the damage produced during transient conditions was calculated with the loads obtained with the models presented in the previous section. Damage was calculated using Miner's rule (Eqn. (4))

$$D = \sum_{i=1}^Z \frac{1}{N_{fi}} \quad (4)$$

where Z is the number of cycles and N_{fi} is the fatigue life for the i -th cycle. The fatigue life for each cycle was calculated by using the Wang-Brown multiaxial fatigue model [12] given by Eqn. (5)

$$\frac{\frac{\Delta\gamma_{\max}}{2} + S\delta\varepsilon_n}{1 + \nu' + S(1 + \nu')} = \frac{\sigma_f' - 2\sigma_{n,mean}}{E} (2N_f)^b + \varepsilon_f' (2N_f)^c \quad (5)$$

where $\Delta\gamma_{\max}$ is the maximum shear strain amplitude for a given reversal and $\delta\varepsilon_n$ is the normal strain excursion between two turning points of the maximum shear strain. The S parameter is a material constant representing sensitivity to crack growth under the normal strain [12]. Here, we used the value 1.38 reported in [12], E is the Young's modulus, $\sigma_{n,mean}$ is the mean normal stress within the loading path, $b, c, \sigma_f', \varepsilon_f'$ are material constants and ν' is the effective Poisson's ratio.

Damage was calculated at the point with the maximum stress concentration. Damage was calculated on planes ranging between $\pm 180^\circ$ with 1° of resolution. This calculation was performed using the corresponding stress components on every plane. Stresses at this critical point were calculated as the measured stress times the corresponding stress concentration factor. The stress concentration factor for axial load was assumed equal to the stress concentration factor for the bending moment.

As a way of validation of the multiaxial fatigue model for the shaft, an approximated $S - N$ uniaxial approach was also performed using the equivalent von Mises stress [15]. For this case, the modification factors were $C_a = 0.76$, $C_b = 0.6$, $C_f = 3.32$, for normal stress, and $C_f = 1.5$ (taken from the FEM results including the notch sensitivity of the material).

Material mechanical properties

The manufacturer of the machine provided the material specification in the Japanese Industrial Standard (JIS). Table 2 presents the international standard equivalency (SAE specification) and the mechanical properties taken from literature [17].

Table 2. Mechanical properties of the material.

| JIS | SAE | S_{ut} (MPa) | S_y (MPa) | ϵ'_f | σ'_f (MPa) | b | c |
|-------|---------|----------------|-------------|---------------|-------------------|--------|-------|
| G3201 | SAE1045 | 671 | 353 | 0.486 | 916 | -0.079 | -0.52 |

RESULTS

Stress measurement

A set of data corresponding to shear and normal stresses at the evaluated power levels, and including start-up and load rejection, is shown in Figure 5. Normal stresses during load rejections were not registered because of technical problems. Each step corresponds to a set of data taken at a given power level during 15 seconds. The number above each step of data corresponds to the generated power value in MW. The transient stresses during the change between power levels are not shown in Figure 5. Both, normal and shear stresses increased with increasing generated power. The maximum shear stress was 45.9 MPa during operation at 100 MW, and the minimum shear stress was -7.73 MPa, which was registered after load rejection where an inversion of the torque occurred when the rotor, with greater inertial moment, tended to drag the runner. The maximum normal stress was 19.98 MPa obtained with the machine working at 100 MW and the minimum was -4.18 MPa during the start-up of the machine. The start-up process occurred in two phases: an initial acceleration of the rotor from rest to a small velocity with negligible shear stress, followed by the acceleration of the rotor to the nominal speed where the shear stress reached a peak value of 9.82 MPa.

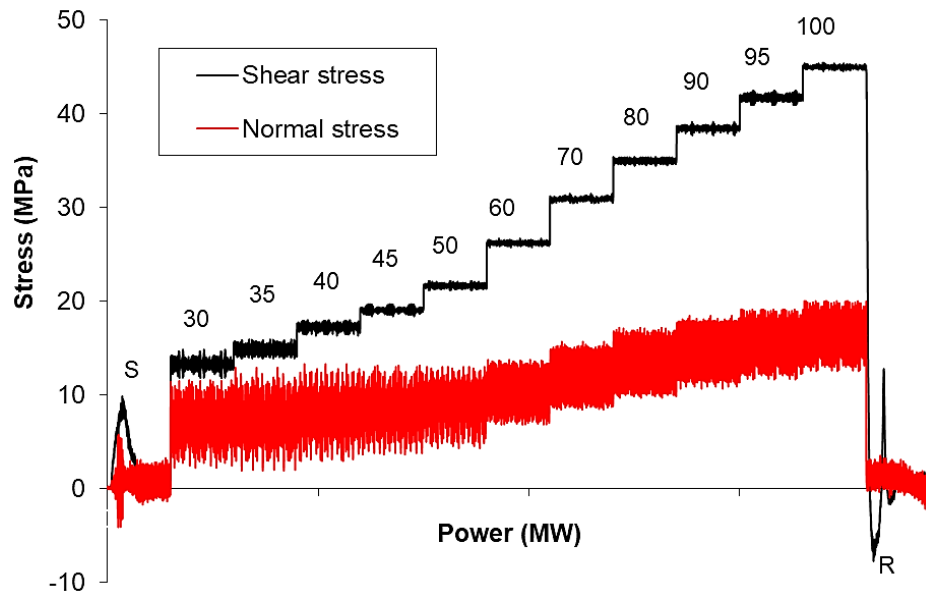


Figure 5. Shear and normal stresses with the machine working at power between 30 and 100 MW. S corresponds to start-up of the machine and R corresponds to load rejection.

For each power level, the stresses consisted of an average value component and a fluctuation component around it. The average values were interpolated to calculate the stresses at those power levels not measured in field test, and then fitted to the power history to obtain the stress history produced by CPL. The fluctuation of stresses was used to calculate the damage per hour due to vibration. Normal stresses were considerably smaller than shear stresses, but normal stresses fluctuated much more, with a frequency equal to the frequency of the rotation of the machine (3 Hz). After filtering the 3 Hz component from the data, the axial force and the bending moment were calculated. Figure 6A shows the average torque and normal force for the evaluated power levels. Average bending moment is not shown since it is approximately zero. The standard deviation for torque, axial force and bending moment is presented in Figure 6B as an indicator of the fluctuation of the data for each power level. The fluctuation of the three loads, torque, axial and bending, increased for power values lower than 60 MW, which corresponded to partial load operation.

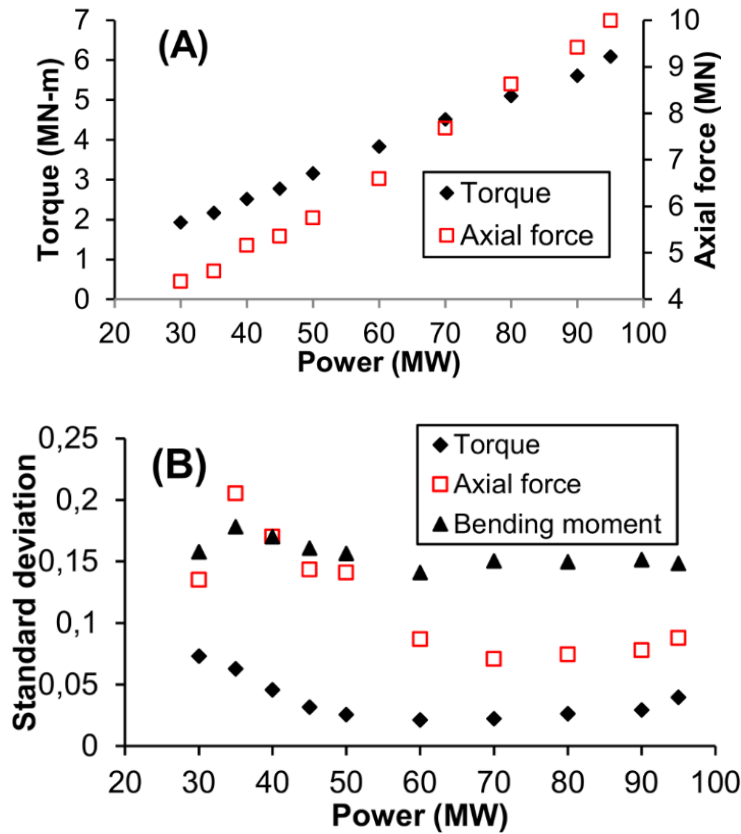


Figure 6. Loads on the shaft: (A) Average torque and axial force as a function of generated power and (B) Standard deviation of torque, axial force and bending moment.

Finite element model results

The region with the highest normal stress concentration was the bell shaped region located at the generator guide bearing where a stress value of 63.75 MPa was obtained (Figure 7). On the other hand, the normal stress on the cylindrical outer surface was 16.77 MPa. With these values, a stress concentration of 3.8 was calculated. The maximum shear stress was found at the same location with a stress concentration factor of 1.67.

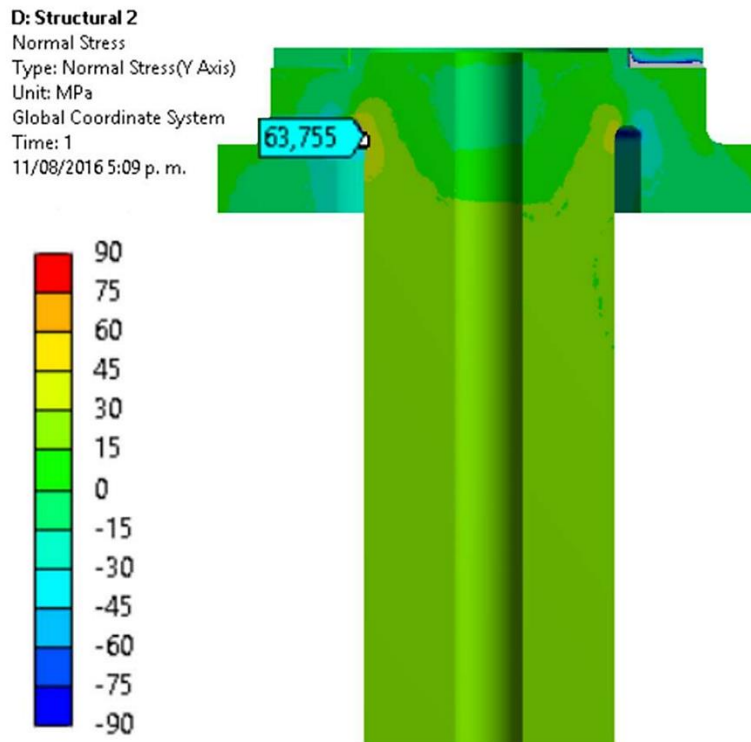


Figure 7. Region of maximum stress concentration of the shaft, corresponding to the transition between the cylindrical part of the shaft, and the generator-bearing region.

Transient condition modelling results

Transient torque at the shaft is presented in Figure 8A for PG failure where it can be noted that, for this kind of failure, the electrical torque is increased up to 2.5-fold with respect to the nominal torque (torque at 100 MW). Meanwhile, PP failure was more severe, producing an increase of approximately 4-fold of the nominal electrical torque (Figure 8B). The torque on the shaft in both cases was only slightly perturbed from the nominal torque, which is due to the high inertial moment of the rotor in comparison with the inertial moment of the runner.

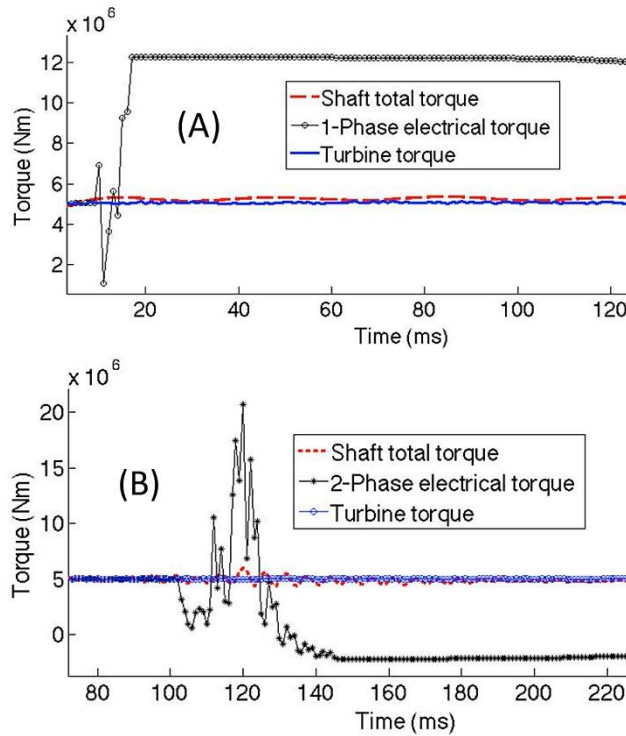


Figure 8. Torque at the shaft produced during transients: (A) phase-to-ground failure and (B) phase-to-phase failure.

Stress history

The generation history during one year of observation is presented in the histogram of Figure 9 where it can be seen that the machine was working mainly at 95 MW.

After interpolation of average measured stresses and the product with the corresponding stress concentration factor and the surface correction factor, a stress history was obtained for each analyzed point. As an example, Figure 10A presents the stress history for the critical point at the generator shaft during one month. In addition, one example of stress fluctuation used to calculate damage per hour due to vibrations is shown in Figure 10B for operation of the machine at 50 MW.

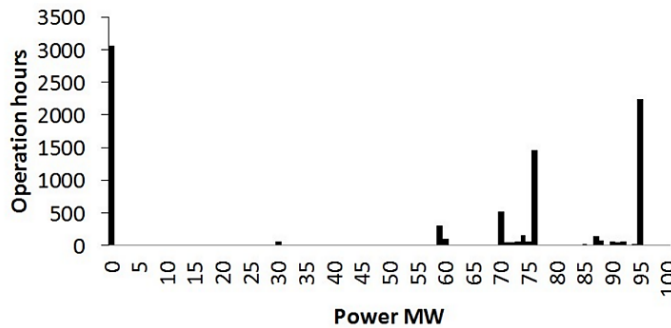


Figure 9. Histogram of the generated power during one year of observation.

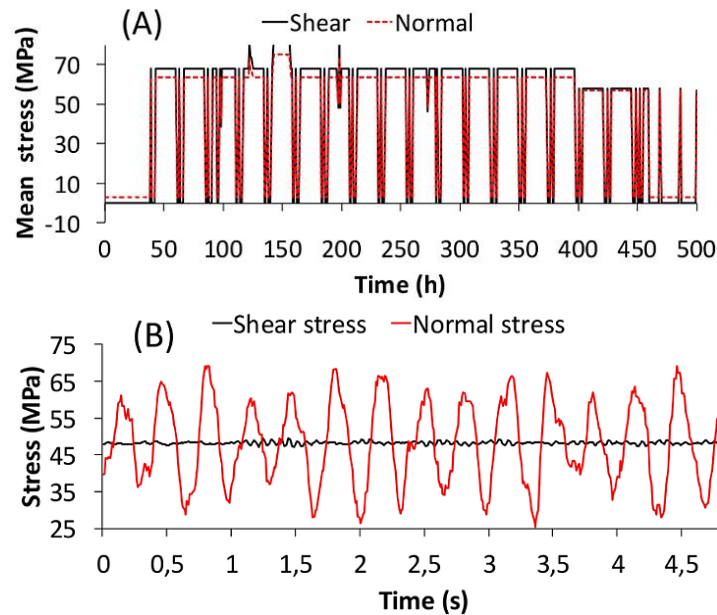


Figure 10. Stresses at the critical point of the shaft: (A) Stress history during one month and (B) Stress fluctuation due to vibration during steady state operation at 50 MW.

Fatigue life results

Damage per hour produced by the vibration of the machine while it was operating in stationary conditions is shown in Figure 11A. The biggest damage per unit of time was produced with the machine working at 40 MW, which correspond to partial load operation. Figure 11B shows the damage due to vibration during the entire year calculated with the histogram from Figure 9. The biggest damage due to vibration (1.593×10^{-6} at an angle of 60°), was produced with the machine working at 95 MW, since the machine was working at this power level most of the time. Important damage was found also at 70 MW, which was the power level with the second largest number of hours of operation. In Figure. 11B, the damage produced due to CPL and the total damage produced during normal operation (N.O.) were also included. Total damage was calculated as the sum of damage due to vibrations plus damage due to CPL. The biggest total damage at the shaft was 9.416×10^{-5} at an angle of 22° . Clearly, CPL produced a much bigger damage than vibrations. Vibrations represented only $\sim 5\%$ of the total damage. Moreover, the angular position of damage due to vibrations was different from that for CPL. With the obtained damage, the calculated life was 106123 years. This results means that the shaft is working under an infinite life regime.

Damage produced by electrical failure is presented in Figure 12 where the previously obtained damage during normal operation (N.O.) was included. Damage produced by electrical failure was not significant in comparison with N.O. damage.

The uniaxial S-N approach using the von Mises equivalent stress and the Goodman criterion showed that for the maximum stress fluctuation, the shaft has an infinite working life since a safety factor of 1.6 was obtained.

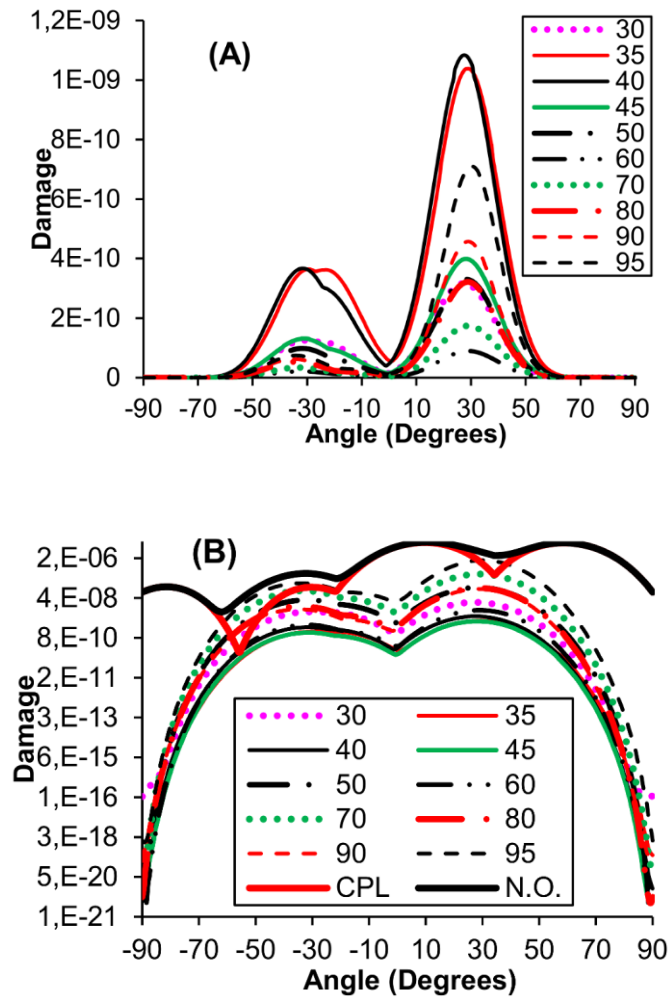


Figure 11. Damage on the shaft as a function of angle: (A) Damage per hour produced by vibration and (B) Damage in log scale during the entire year produced by vibrations, change of power level (CPL), and total damage during normal operation (N.O.). The biggest damage was $9.416e-6$ at an angle of 11° .

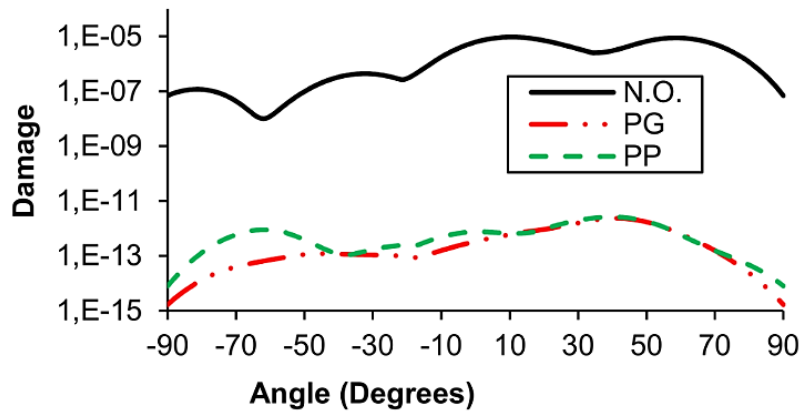


Figure 12. Damage on the shaft during one year as a function of angle produced with the presence of failures: N.O.) damage during one year of normal operation without failures, PG) damage due to one phase to ground failure, PP) damage due to one phase-to-phase failure.

DISCUSSION

Fatigue life analysis using the Wang-Brown multiaxial fatigue approach was performed on the shaft of a 100 MW hydro-generator. To the best of our knowledge, this is the first study where fatigue life was evaluated using a multiaxial approach, with measured stresses under actual working conditions, and using the actual load history.

Measured stress showed a higher fluctuation of torque, axial load and bending moment, while the machine was operating at partial load (between 30% and 60% of full load) than when operating at higher loads. This behavior has been typically observed on Francis turbines and is produced by the von Karman Vortex at the vanes and the Vortex Rope at the draft tube [18, 19]. This high fluctuation produces important fluctuating stresses that may produce fatigue failure on structural elements of the machine [20]. For that reason, companies try to avoid operation at partial load or implement strategies to reduce vibration such as air injection to the stay vanes or to the draft tube [18, 20, 21].

Synchronization of the machine with the network did not produce any appreciable peak of normal or shear stress. This is probably due to the rotor high moment of inertia, making it to behave as flywheel absorbing the sharp peaks of electrical torque and suppressing the effect of those peaks upon the shaft. The same reason may explain the lack of high torsional vibrations on the shaft after load rejection.

Models of PG and PP failures gave peaks of torque considerably smaller than those reported in previous studies [6, 16]. The reason for the difference may be again the greater inertial moment of the rotor in comparison with the turbine and the fact that in this study the model of failure was coupled with the turbine-penstock dynamic model. A long-term torque monitoring system is needed on the machine to register data during a failure and corroborate the results of the model.

The critical point at the shaft was found to be working at an infinite life regime even if one electrical failure occurs per year. During normal operation, the CPL produced a greater damage than the vibrations during operation at steady state.

The main limitations of this work were related to the mechanical properties of the material used for the calculations since they were taken from literature as the actual material properties of the shaft are unknown. The endurance limit needed for the uniaxial approach was assumed to be $0.5S_{ut}$. However, that value may be as low as $0.35S_{ut}$, which significantly affects the calculated fatigue life of the element. Therefore, the actual mechanical properties of the material should be identified to improve the accuracy of the calculations performed in this work.

The fatigue analysis for the shaft was performed assuming that the nominal stresses at the upper bearing (near the critical point) were the same as the measured stresses. However, normal stress measurements at several points along the shaft are needed to establish a more accurate model for the shaft. Even though fatigue analysis was performed with the measured stress values, it is necessary to be aware that those stresses may change in the long term, for example, due to wear on the seals of the runner, which may increase the leak of water to the top of the runner, increasing the axial force. This increase in axial force may significantly accelerate fatigue failures. Therefore, a periodic monitoring of loads is recommended. Other sources of error for the present study lie in the fact that stresses were not measured at every power level of the machine, and for the fatigue life calculations, the average value was interpolated. Additionally, the vibrations for those power levels where strains were not measured were assumed to be equal to the measured values at the power level immediately above. However, damage produced by these fluctuations was small. Therefore, the error produced by this assumption should be negligible.

CONCLUSIONS

Normal and axial stresses on the shaft were found to consist of an average value that increased with increasing generated power and a fluctuation of stresses around the average value due to vibration, which were highest during partial load operation. The frequency of the main fluctuation of normal stress was equal to the frequency of the machine rotation, probably because that fluctuation is produced by a bending moment on the shaft. Synchronizations of the machine with the network and load rejection did not produce high torsional vibrations. This is probably because the rotor's high moment of inertia make it work as flywheel, absorbing the sharp peaks of transient phenomena.

The shaft was found to be working at infinite fatigue life. However, the actual mechanical properties of the material need to be measured in order to improve the accuracy of the fatigue life calculation. On the shaft, CPL produced greater damage than vibration during steady state operation.

ACKNOWLEDGEMENTS

This work was supported by the vice-presidency of research from Universidad del Valle, grant number CI 806. Authors also thank CELSIA-EPISA (Empresa de Energia del Pacifico) for the support given to this research.

REFERENCES

- [1] Momcilovic D, Odanovic Z, Mitrovic R, Atanasovska I, Vuherer T. Failure analysis of hydraulic turbine shaft. *Engineering Failure Analysis*. 2012;20:54-66.
- [2] Zhang Z, Yin Z, Han T, Tan A. Fracture analysis of wind turbine main shaft. *Engineering Failure Analysis*. 2013;34:129-139.
- [3] Chyn C, Wu RC, Tsao TP. Torsional fatigue of turbine-generator shaft owing to network faults. *IEE Proceedings- Generation, Transmission and Distribution*. 1996;143(5):479-486.
- [4] Joyce JS, Kulig T. Torsional fatigue of turbine-generator shaft caused by different electrical system faults and switching operations. *IEEE Transactions on Power Apparatus and Systems*. 1987;97(5):1965-1977.
- [5] Mitsche JV, Rusche PA. Shaft torsional stress due to asynchronous fault synchronization. *IEEE Transactions on Power Apparatus and Systems*. 1980;99(5):1864-1870.
- [6] Xie X, Dong Y, Han Y. Online estimation of turbine-generator shaft fatigue loss-of-life caused by subsynchronous resonance. *Electric Power Systems Research*. 2012;92:171-179.
- [7] Dorji U, Ghomashchi R. Hydro turbine failure mechanisms: an overview. *Engineering Failure Analysis*. 2014;44:136-147.
- [8] Liu X, Lou Y, Wang Z. A review on fatigue damage mechanism in hydro turbines. *Renewable and Sustainable Energy Reviews*. 2016;54:1-14.
- [9] Gagnon M, Tahan A, Bocher P, Thibault, D. A probabilistic model for the onset of High Cycle Fatigue (HCF) crack propagation: Application to hydroelectric turbine runner. *International Journal of Fatigue*. 2013;47:300-307.
- [10] Casanova F, Mantilla C, Fatigue failure of the bolts connecting a Francis turbine with the shaft. *Engineering Failure Analysis*. 2018;90:1-13.
- [11] Wang CH, Brown MW. Life prediction techniques for variable amplitude multiaxial fatigue – Part 1: Theories. *Journal of Engineering Materials and Technology*. 1996;118(3):367-370.
- [12] Kirschbaum HS. Transient electrical torques of turbine generators during short circuits and synchronizing. *IEEE Transactions*. 1945;64(2):67-70.
- [13] Mantilla CA, Valdés JA. Development of an elastic-water column model for penstock including water hammer effect and optimization with field test based results. In: 11th Latin American Congress on Electricity Generation and Transmission CLAGTEE "Bioenergy for Electricity Generation and Ecological Issues in Power Plants", Sao Jose dos Campos, Brazil; 8-11 November, 2015.
- [14] Baruh H. *Analytical Dynamics*, 2nd ed. Boston: McGraw-Hill, 1999.
- [15] Norton RL. *Machine design an integrated approach*, 4th ed. Mexico: Pearson Education, 1998.
- [16] Joyce JS, Lambrecht D. Status of evaluating the fatigue of large steam turbine-generator caused by electrical disturbances. *IEEE Transactions on Power Apparatus and Systems*. 1980;99(1):111-119.
- [17] Stephens RI, Stephens RR, Fuchs HO. *Metal fatigue in engineering*, 2nd ed. New York: John Wiley & Sons, Inc, 2001.

- [18] Qian Z, Yang J, Huai W. Numerical simulation and analysis of pressure pulsation in Francis hydraulic turbine with air admission. *Journal of Hydrodynamics, Serie B.* 2007;19:467-472.
- [19] Nicolet C, Arpe J, Avellan F. Identification and modelling of pressure fluctuations of a Francis turbine scale model at partial load operation. In: 22nd LAHR symposium on Hydraulic Machinery and Systems, Stockholm, Sweden, 29 June - 2 July, 2004.
- [20] Casanova F, Mantilla C. Experimental analysis of the vibration on the draft tube of a Francis hydraulic turbine during operation at different power levels. *Revista Facultad de Ingeniería Universidad de Antioquia.* 2010;55:90-98.
- [21] Gunter, H., Zanutto, J.C., and Ponge-Ferreira, W. Hydraulic power plant machine dynamic diagnosis. *Shock and Vibration.* 2006;13:409-427.